SCIENCE CHINA
Technological Sciences

July 2011 Vol.54 No.7: 1841–1848
doi: 10.1007/s11431-011-4358-4

# Identification and robust limit-cycle-oscillation analysis of uncertain aeroelastic system

DAI YuTing*, WU ZhiGang & YANG Chao

*School of Aeronautic Science and Engineering, Beijing University of Aeronautics and Astronautics, Beijing 100191, China*

Received July 23, 2010; accepted January 17, 2011; published online April 14, 2011

Model uncertainty directly affects the accuracy of robust flutter and limit-cycle-oscillation (LCO) analysis. Using a data-based method, the bounds of an uncertain block-oriented aeroelastic system with nonlinearity are obtained in the time domain. Then robust LCO analysis of the identified model set is performed. First, the proper orthonormal basis is constructed based on the on-line dynamic poles of the aeroelastic system. Accordingly, the identification problem of uncertain model is converted to a nonlinear optimization of the upper and lower bounds for uncertain parameters estimation. By replacing the identified memoryless nonlinear operators by its related sinusoidal-input describing function, the Linear Fractional Transformation (LFT) technique is applied to the modeling process. Finally, the structured singular value ($\mu$) method is applied to robust LCO analysis. An example of a two-degree wing section is carried out to validate the framework above. Results indicate that the dynamic characteristics and model uncertainties of the aeroelastic system can be depicted by the identified uncertain model set. The robust LCO magnitude of pitch angle for the identified uncertain model is lower than that of the nominal model at the same velocity. This method can be applied to robust flutter and LCO prediction.

**aeroelasticity, robust, identification, uncertainty, structured singular value $\mu$, limit-cycle-oscillation**

**Citation:** Dai Y T, Wu Z G, Yang C. Identification and robust limit-cycle-oscillation analysis of uncertain aeroelastic system. Sci China Tech Sci, 2011, 54: 1841–1848, doi: 10.1007/s11431-011-4358-4

## 1 Introduction

Flutter and limit-cycle oscillation (LCO) have been prevalent aeroelastic problems on several aircrafts. Traditional flutter and LCO analysis are based on the nominal dynamics with the known aerodynamic and structural parameters. By introducing enough flutter safety margin, aircrafts could avoid experiencing flutter/limit-cycle oscillation within flight regimes, although some kinds of nonlinearities and uncertainties still exist. Since the computational and experimental methods have been improved significantly, flutter and LCO calculation are more accurate than before. However, the same flutter margin is still employed nowadays due to the lack of quantification of complicated nonlinearities and uncertainties. Questions arise: will flutter and LCO occur when various dynamic uncertainties are considered? In the previous studies, robust stability method is proved to be an effective tool in uncertainty quantification for the linear time invariant (LTI) system [1]. Robust flutter analysis, based on the structured singular value ($\mu$) method [2–5], concerns the minimum stability margin of aircraft, considering all kinds of uncertainties within flight boundary. The focus of robust flutter analysis *a prior* to this work is concentrated on physical modeling of uncertainties and robust flutter boundary prediction. In these researches, the uncertainty type and bound are assumed to be known and are then verified in a linear framework. However, the physical modeling and verification of nonlinearity are still a hard task due to its complicated mechanism. Without proper es-

*Corresponding author (email: yutingdai@ase.buaa.edu.cn)

timation of uncertainty bound and nonlinearity, the robust flutter or LCO prediction results may be misleading. In contrast to the previous state-of-the-art LCO analysis methodology that employs high-level computational fluid dynamics methods with built-in nonlinear models, alternatively, some data-based identification methods for linear and nonlinear models were applied to the identification of the online aeroelastic dynamics [6–9]. While the identified nominal model should introduce additional physical modeling of uncertainty to conduct flutter and LCO prediction because the nominal model may not consider about the model's error itself. The goal of the current study is to investigate the LCO phenomenon based on an identification framework for control-oriented model set without sufficiently physical modeling.

In this current work, the data-based identification framework for block-oriented model is proposed to investigate the LCO phenomenon of aeroelastic system with consideration of nonlinearity and uncertainties. With proper orthonormal basis tuned with on-line aeroelastic poles, the uncertain model identification problem is converted to the one of estimating the upper and lower bounds of uncertain parameters. The one-step identification method for Hammerstein model is presented to solve the parameter bounds directly. And then the describing function method and LFT technique are applied to robust LCO analysis. Finally, the identification and LCO analysis framework are validated by a two-dimensional wing section aeroelastic system.

## 2 Model set identification for the uncertain aeroelastic system

### 2.1 Problem formulation

An aeroelastic system that accounts for unmodeled dynamics can be described by the following equation [10]:

$$\boldsymbol{M}\ddot{x} + \boldsymbol{C}\dot{x} + \boldsymbol{K}x - \boldsymbol{F}u = \boldsymbol{X}(\boldsymbol{\upsilon}), \tag{1}$$

where $\boldsymbol{M}, \boldsymbol{C}, \boldsymbol{K} \in \boldsymbol{R}^{n_x \times n_x}$ describe the structural general mass, damping, and stiffness matrix, respectively, $\boldsymbol{F} \in \boldsymbol{R}^{n_x \times n_u}$ is the external force matrix. In this equation, $\boldsymbol{x} \in \boldsymbol{R}^{n_x}$ stands for the modal displacement vector, and $\boldsymbol{u} \in \boldsymbol{R}^{n_u}$ is the input vector. The additional signal $\boldsymbol{\upsilon}$ is a linear combination of the states and inputs. And the function on the right side of eq. (1), $\boldsymbol{X}(\boldsymbol{\upsilon})$, represents an unknown and nonlinear contribution to the dynamics. Considering a formulation that the nonlinear dynamics is only related to status vector, the single-input-single-output model considered in this study can be expressed by the Block-oriented nonlinear diagram illustrated in Figure 1 [10].

As shown in Figure 1, the system is now represented as a nonlinear feedback formulation added on an inaccurate linear part. The above model, which is applied to represent the

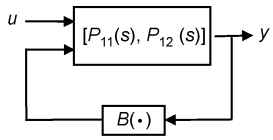


**Figure 1** Block-oriented system in feedback with nonlinearity.

phenomenon of output multiplicity, presents a clearly visible block structure of a memoryless nonlinearity together with a LTI system in a feedback connection. In this Block-oriented model, $P_{11}(s)$, $P_{12}(s)$ represent the LTI part of the aeroelastic system, and $B(\upsilon)$ is a reflection of the nonlinearity operation. In the linear part, $P_{11}(s)$ can be derived based on the physical modeling of the aeroelastic system. However, it may be not so accurate, so the feedback nonlinear model is added to depict this modeling error. In the identification procedure, we assume that the linear and nonlinear parts $P_{12}(s)$, $B(\upsilon)$ can be represented by a set of known basis functions, which are given by eqs. (2) and (3):

$$P_{12}(s) = \sum_{i=1}^{r} \alpha_i L_i(s), \tag{2}$$

$$B(\upsilon) = \sum_{i=1}^{n} \beta_i f_i(\upsilon), \tag{3}$$

where $L_i(s)$ is a rational orthonormal basis function of linear part $P_{12}(s)$; $f_i(\upsilon)$ represents the nonlinear basis function of $B(\upsilon)$; $r$ and $n$ represent the number of linear and nonlinear bases, respectively; parameters $\alpha_i$, $\beta_i \in \boldsymbol{R}$ are the unknown coefficients of linear and nonlinear model bases. The upper and lower bounds of these coefficients illustrate the following model set:

$$\boldsymbol{\Delta}_\alpha = \left\{ \boldsymbol{\alpha} : \alpha_i^{\mathrm{l}} \leqslant \alpha_i \leqslant \alpha_i^{\mathrm{u}}, i = 1, \cdots, r, \boldsymbol{\alpha} \in \boldsymbol{R}^{1\times r} \right\}, \tag{4}$$

$$\boldsymbol{\Delta}_\beta = \left\{ \boldsymbol{\beta} : \beta_i^{\mathrm{l}} \leqslant \beta_i \leqslant \beta_i^{\mathrm{u}}, i = 1, \cdots, n, \boldsymbol{\beta} \in \boldsymbol{R}^{1\times n} \right\}, \tag{5}$$

where the superscripts l and u represents the lower bounds and the upper bounds of the coefficients for the model set.

As presented above, the identification problem of uncertain model set shown in Figure 1 can be concluded as: the unknown upper and lower bound parameters $\boldsymbol{\alpha}^{\mathrm{u}}$, $\boldsymbol{\alpha}^{\mathrm{l}}$, $\boldsymbol{\beta}^{\mathrm{u}}$, $\boldsymbol{\beta}^{\mathrm{l}}$ of the uncertain model set $\boldsymbol{\Delta}_\alpha$, $\boldsymbol{\Delta}_\beta$ are estimated based on the physical model $P_{11}(s)$ and $N$-point data records of the measured input-output signals $u$, $y$ in the time domain in a flight test or a wind tunnel experiment. After the identification procedure, the model set should characterize the aeroelastic dynamics.

### 2.2 Identification method for uncertain model set

We consider the single-input-single-output situation in Figure 1. Consequently, in the Block-oriented model, the nonlinear gain maps the output sequence into the intermediate

sequence. Together with the input signal, it is mapped through the different linear parts to produce model's output. Considering the parametric expressions of eqs. (2) and (3), the output of the model for every input signal $u(k)$ in the time domain is given by

$$\begin{aligned}\bar{y}(k) &= P_{11}(s)u(k)+\sum_{i=1}^{r}\alpha_i L_i(s)\left(\sum_{j=1}^{n}\beta_j f_j(y(k))\right)\\ &= P_{11}(s)u(k)+\sum_{i=1}^{r}\sum_{j=1}^{n}\alpha_i\beta_j L_i(s)f_j(y(k)).\end{aligned} \tag{6}$$

In eq. (6), we assume that

$$\begin{aligned}\boldsymbol{\Theta}(k) = [&L_1(s)f_1(y(k)),\cdots,L_1(s)f_n(y(k)),\cdots,\\ &L_r(s)f_1(y(k)),\cdots,L_r(s)f_n(y(k))]^{\mathrm{T}},\end{aligned} \tag{7}$$

where $\boldsymbol{\Theta}(k)\in\boldsymbol{R}^{rn\times 1}$. The unknown parameter vector is denoted as $\boldsymbol{\theta}\in\boldsymbol{R}^{rn\times 1}$. It is written as

$$\boldsymbol{\theta} = [\alpha_1\beta_1,\cdots,\alpha_1\beta_n,\alpha_2\beta_1,\cdots,\alpha_r\beta_n]^{\mathrm{T}}. \tag{8}$$

And $\bar{e}(k)$ is used to represent the difference between the output of the real system and that of the linear model $P_{11}(s)$. That is

$$\bar{e}(k) = \bar{y}(k) - P_{11}u(k). \tag{9}$$

Then eq. (6) can be rewritten as a linear regression of the unknown parameter vector:

$$\bar{e}(k) = \boldsymbol{\theta}^{\mathrm{T}}\boldsymbol{\Theta}(k). \tag{10}$$

Assume that

$$\begin{aligned}\boldsymbol{\Theta}^{+}(k) &= \max[\boldsymbol{\Theta}(k),0],\\ \boldsymbol{\Theta}^{-}(k) &= \min[\boldsymbol{\Theta}(k),0].\end{aligned} \tag{11}$$

The two-step identification algorithm, proposed by Biagiola [11, 12], first estimates the lower bound $\boldsymbol{\theta}^{\mathrm{l}}$ and the upper bound $\boldsymbol{\theta}^{\mathrm{u}}$ of the intermediate model set $\boldsymbol{\Delta}_\theta$. Then the model set $\boldsymbol{\Delta}_\alpha$, $\boldsymbol{\Delta}_\beta$ is obtained by solving a nonlinear optimization. This algorithm needs the first-step model set as subset of that in the second step, which is to satisfy the requirement that the experimental data $y(k)$ can be covered by the output of the model set $\boldsymbol{\Delta}_\alpha$, $\boldsymbol{\Delta}_\beta$. It would bring about conservativeness in the parameters' bound. In this section, intermediate model set $\boldsymbol{\Delta}_\theta$ is not estimated. Alternatively, the parameter bounds of model set $\boldsymbol{\Delta}_\alpha$, $\boldsymbol{\Delta}_\beta$ are identified directly. The optimization objective indicates the error bound of the model's output, instead of the unknown parameters, which is given by

$$\min \sum_{k=1}^{N}(\bar{e}_{\max}(k)-\bar{e}_{\min}(k)), \tag{12}$$

s.t.

$$\begin{cases}\max(\alpha_i^{m1}\boldsymbol{\beta}^{m2})\boldsymbol{\Theta}^{+}(k)+\min(\alpha_i^{m1}\boldsymbol{\beta}^{m2})\boldsymbol{\Theta}^{-}(k)\geqslant e(k),\\ \min(\alpha_i^{m1}\boldsymbol{\beta}^{m2})\boldsymbol{\Theta}^{+}(k)+\max(\alpha_i^{m1}\boldsymbol{\beta}^{m2})\boldsymbol{\Theta}^{-}(k)\leqslant e(k),\\ m1,m2=\mathrm{l},\mathrm{u};\\ \alpha_i^{\mathrm{l}}\leqslant\alpha_i^{\mathrm{u}},\beta_j^{\mathrm{l}}\leqslant\beta_j^{\mathrm{u}},i=1,\cdots r,j=1,\cdots,n.\end{cases} \tag{13}$$

The constraints in eq. (13) can be interpreted from a graphical point of view as shown in Figure 2.

In Figure 2, Point $A(k)$ represents the left inequality of the first constraint in eq. (13), that is, $A(k)=[\boldsymbol{\Theta}^{-}(k), \boldsymbol{\Theta}^{+}(k)]\begin{bmatrix}\boldsymbol{\theta}^{\mathrm{l}}\\ \boldsymbol{\theta}^{\mathrm{u}}\end{bmatrix}$. Similarly, Point $B(k)$ illustrates the second one.

These two constraints mean that for a certain input signal $u(k)$, the error signal $e(k)$ should be covered by the maximum and the minimum output values of the model set $\boldsymbol{\Delta}_\alpha$, $\boldsymbol{\Delta}_\beta$. The third inequality of eq. (13) means that each of the lower bound parameters should be less than that of the upper bound parameters of the model set. From the constraint in eq. (13), the one-step identification algorithm is an optimization with nonlinear constraint. The calculating procedure is outlined: The two-step least square method and SVD decomposition method [6] are applied to the estimation of the nominal parameters $\boldsymbol{\alpha}_m$, $\boldsymbol{\beta}_m$ for the Block-oriented model. These nominal parameters are set as the initial values for uncertain model set identification by iterative method. The upper and lower bounds of the model set $\boldsymbol{\Delta}_\alpha$, $\boldsymbol{\Delta}_\beta$ are solved by sequential quadratic programming (SQP) method.

The indicative function coincident with objective function in eq. (12) is given by

$$F_e = \frac{\sum_{k=1}^{N}\left|(\bar{e}_{\max}(k)-\bar{e}_{\min}(k))\right|}{\sum_{k=1}^{N}\left|\bar{e}(k)\right|}. \tag{14}$$

Obviously, smaller indicative function value $F_e$ produces less conservativeness of the model set when the constraints in eq. (13) are guaranteed.

### 2.3 Basis function construction

The orthonormal basis of linear model $P_{12}(s)$ and the basis of the nonlinear gain $B(v)$ are presented in this section.

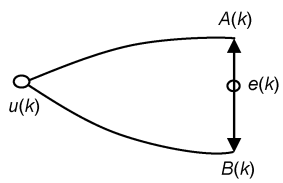


**Figure 2** Graphical representation of uncertain model set identification.

Firstly, we assume that the transfer function matrix of the linear aeroelastic dynamics can be represented parametrically by a set of orthonormal basis function $L_i(s)$. And the rational orthonormal basis obtained from a series of scalar all-pass filters is constructed using *a-prior* knowledge of the aeroelastic dynamics. Most of the linear aeroelastic problems are based on the modal base assumption, since the important modal dynamics such as natural frequency, damping ratio can be obtained by the ground vibration test. As we know that the natural frequencies of elastic structures are relatively low. However, the FIR filter is not suitable to constructing the basis of true dynamics with low modes, because the model order should be very large to provide an accurate approximation to the true dynamics. Meanwhile, for the similar reason, standard Kautz and Laguerre filters can only utilize the main dominant poles but not most of the important poles, more orders of these filters are needed to satisfy error limitations [12–14]. Hence, the essential idea of the basis construction is to employ the important poles of the natural modes as many as possible [15]. Then we assume that the impulse response of the true dynamics can be approximated by linear combination of this orthonormal basis tuned with the elastic poles of the aeroelastic system. The poles in the frequency domain are denoted as $p_i$, and the sample time interval is $T_s$. Then the poles in the discrete $z$ domain can be expressed as $\xi_i = e^{p_i T_s}$. Since the poles of the aeroelastic dynamics without rigid modes are complex, that is $\xi_i=\xi^*_{i+1}$, $i$=1,…3,…$r$–1, then the $i$, $i$+1 orthonormal bases using all-pass filters are given as [12]

$$\begin{aligned} L_i(z) &= \frac{\sqrt{(1-\eta_i^2)(1-|\xi_i|^4)}}{z^2-2\times Re(\xi_i)z+|\xi_i|^2}\prod_{k=0}^{i-1}\left(\frac{1-\xi_k^* z}{z-\xi_k}\right), \\ L_{i+1}(z) &= \frac{\sqrt{(1-|\xi_i|^4)}\times(z-\eta_i)}{z^2-2\times Re(\xi_i)z+|\xi_i|^2}\prod_{k=0}^{i-1}\left(\frac{1-\xi_k^* z}{z-\xi_k}\right), \end{aligned} \tag{15}$$

where $\eta_i = \dfrac{2Re(\xi_i)}{1+|\xi_i|^2}$.

Polynomial basis to construct the nonlinear memoryless map is selected as below

$$f_j(\upsilon) = \upsilon^j, j = 1,\cdots,n. \tag{16}$$

Note that we choose the polynomial functions to represent the nonlinear dynamics, but they can be cubic-spline, sigmoid, or radial basis functions as well. It depends on our choice with different problems.

## 3 Robust LCO analysis for uncertain aeroelastic system

After obtaining the upper and lower bound parameters $\boldsymbol{\alpha}^{\mathrm{u}}$, $\boldsymbol{\alpha}^{\mathrm{l}}$, $\boldsymbol{\beta}^{\mathrm{u}}$, $\boldsymbol{\beta}^{\mathrm{l}}$ for the uncertain Block-oriented model set $\boldsymbol{\Delta}_\alpha$, $\boldsymbol{\Delta}_\beta$ in the sections above, the following parametric expressions are obtained from eqs. (4) and (5):

$$\begin{gathered} \left\{\boldsymbol{\Delta}_\alpha : \boldsymbol{\alpha} = \boldsymbol{\alpha}_0 + \boldsymbol{\delta}_\alpha ; \boldsymbol{\Delta}_\beta : \boldsymbol{\beta} = \boldsymbol{\beta}_0 + \boldsymbol{\delta}_\beta\right\} \\ \left|\boldsymbol{\delta}_\alpha\right| \leqslant \boldsymbol{\delta}_{\alpha\max}, \left|\boldsymbol{\delta}_\beta\right| \leqslant \boldsymbol{\delta}_{\beta\max}, \end{gathered} \tag{17}$$

$$\begin{aligned} \boldsymbol{\alpha}_0 &= \frac{1}{2}(\boldsymbol{\alpha}^{\mathrm{u}} + \boldsymbol{\alpha}^{\mathrm{l}}), \boldsymbol{\delta}_{\alpha\max} = \frac{1}{2}(\boldsymbol{\alpha}^{\mathrm{u}} - \boldsymbol{\alpha}^{\mathrm{l}}), \\ \boldsymbol{\beta}_0 &= \frac{1}{2}(\boldsymbol{\beta}^{\mathrm{u}} + \boldsymbol{\beta}^{\mathrm{l}}), \boldsymbol{\delta}_{\beta\max} = \frac{1}{2}(\boldsymbol{\beta}^{\mathrm{u}} - \boldsymbol{\beta}^{\mathrm{l}}), \end{aligned} \tag{18}$$

where $\boldsymbol{\alpha}_0$, $\boldsymbol{\delta}_\alpha$, $\boldsymbol{\delta}_{\alpha\max} \in \boldsymbol{R}^{1\times r}$, $\boldsymbol{\beta}_0$, $\boldsymbol{\delta}_\beta$, $\boldsymbol{\delta}_{\beta\max} \in \boldsymbol{R}^{1\times n}$. $\boldsymbol{\alpha}_0$, $\boldsymbol{\beta}_0$ are the nominal parameters of the model set. The nonlinear Block-oriented model illustrated in Figure 1 can be described by Figure 3.

In Figure 3, $\boldsymbol{L}(s)=[L_1,\ldots,L_r]^{\mathrm{T}}$, and $L_i$ represents the $i$th linear orthonormal basis. We use the polynomial functions to represent the feedback nonlinearity, that is $\boldsymbol{f}(\upsilon)=[\upsilon^1, \upsilon^2,\ldots, \upsilon^n]^{\mathrm{T}}$. By replacing the identified memoryless operator by their related sinusoidal-input describing function to model the first harmonic gain, the nonlinear basis in the time domain can be transformed to its frequency domain near its critical instability point. The describing function method relies on the assumption that only the fundamental harmonic dynamics is significant. This assumption is often valid in aeroelastic systems. The describing function for the polynomial basis in the time domain is given by [16]

$$N_i(X) = \frac{2}{\sqrt{\pi}} X^{i-1} \frac{\Gamma\left[\dfrac{i+2}{2}\right]}{\Gamma\left[\dfrac{i+3}{2}\right]}, \text{ where } i > 2, \tag{19}$$

where $X$ represents the magnitude of the flapping angle and $\Gamma[\cdot]$ is the gamma function, and $\Gamma(1/2) = \sqrt{\pi}$.

Note that $\boldsymbol{N}(X)=[N_1(X),\ldots,N_n(X)]^{\mathrm{T}}$. The output of the model set indicated in Figure 3 is written as

$$y = P_{11}(s)u + \left[\boldsymbol{\alpha}_0\boldsymbol{L}(s) + \boldsymbol{\delta}_\alpha\boldsymbol{L}(s)\right][\boldsymbol{\beta}_0\boldsymbol{N}(X) + \boldsymbol{\delta}_\beta\boldsymbol{N}(X)]y. \tag{20}$$

The introduced virtual signals $\boldsymbol{n}_1$, $\boldsymbol{q}_1 \in \boldsymbol{R}^{r\times 1}$; $\boldsymbol{n}_2$, $\boldsymbol{q}_2 \in \boldsymbol{R}^{n\times 1}$ satisfy the following relationship:

$$\begin{aligned} \boldsymbol{q}_1 &= \frac{1}{1-\boldsymbol{\alpha}_0\boldsymbol{L}\boldsymbol{\beta}_0\boldsymbol{N}} \times (\boldsymbol{L}\boldsymbol{\beta}_0\boldsymbol{N}\boldsymbol{W}_\alpha\boldsymbol{n}_1 + \boldsymbol{L}\boldsymbol{W}_\beta\boldsymbol{n}_2 + \boldsymbol{L}\boldsymbol{\beta}_0\boldsymbol{N}P_{11}u), \\ \boldsymbol{q}_2 &= \frac{1}{1-\boldsymbol{\alpha}_0\boldsymbol{L}\boldsymbol{\beta}_0\boldsymbol{N}} \times \left[\boldsymbol{N}\boldsymbol{W}_\alpha\boldsymbol{n}_1 + \boldsymbol{N}\boldsymbol{\alpha}_0\boldsymbol{L}\boldsymbol{W}_\beta\boldsymbol{n}_2 + \boldsymbol{N}P_{11}u\right], \\ \boldsymbol{n}_1 &= \boldsymbol{\Lambda}_\alpha\boldsymbol{q}_1, \\ \boldsymbol{n}_2 &= \boldsymbol{\Lambda}_\beta\boldsymbol{q}_2, \end{aligned} \tag{21}$$

where $\boldsymbol{W}_\alpha \in \boldsymbol{R}^{1\times r}$, $\boldsymbol{W}_\beta \in \boldsymbol{R}^{1\times n}$, which represent the weighting matrixes for uncertainties $\boldsymbol{\delta}_\alpha$ and $\boldsymbol{\delta}_\beta$, respectively, and scale the perturbations such that the uncertainty parameters $\boldsymbol{\delta}_\alpha$ and $\boldsymbol{\delta}_\beta$ belong to the set $\|\boldsymbol{\Delta}\|_\infty \leqslant 1$. Then, the uncertain models shown in Figure 3 can be transformed into the feedback

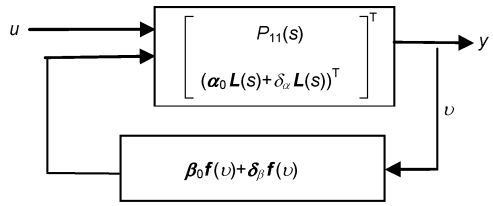


**Figure 3** Block-oriented model with parameters' uncertainties.

models shown in Figure 4, based on a Linear Fractional Transformation (LFT) framework. The LFT model is written as

$$\boldsymbol{M}(s,X)=\frac{1}{1-\boldsymbol{\alpha}_0\boldsymbol{L}\boldsymbol{\beta}_0\boldsymbol{N}}\times\left[\begin{array}{cc|c}\boldsymbol{L}\boldsymbol{\beta}_0\boldsymbol{N}\boldsymbol{W}_\alpha & \boldsymbol{L}\boldsymbol{W}_\beta & \boldsymbol{L}\boldsymbol{\beta}_0\boldsymbol{N}P_{11}\\ \boldsymbol{N}\boldsymbol{W}_\alpha & \boldsymbol{N}\boldsymbol{\alpha}_0\boldsymbol{L}\boldsymbol{W}_\beta & \boldsymbol{N}P_{11}\\ \hline \boldsymbol{W}_\alpha & \boldsymbol{\alpha}_0\boldsymbol{L}\boldsymbol{W}_\beta & P_{11}\end{array}\right]. \quad (22)$$

The robust stability theorem indicates that the robust stability of the system as shown in Figure 4 is only related to the matrix $\boldsymbol{M}_{11}$ in the LFT framework, based on the structured singular value method [3].

When the nominal system remains stable, the loop shown in Figure 4 is well-posed and internally stable for all $\boldsymbol{\Delta}=\begin{bmatrix}\boldsymbol{\Lambda}_\alpha & \\ & \boldsymbol{\Lambda}_\beta\end{bmatrix}$ with $\|\boldsymbol{\Delta}\|_\infty\leqslant 1$ if and only if

$$\sup_{\omega\in\boldsymbol{R}}\mu\left[\boldsymbol{M}_{11}(\omega)\right]<1. \quad (23)$$

After the identification and modeling procedures, the robust limit-cycle-oscillation analysis is performed as follows: at a specified velocity, increasing the magnitude of the pitch angle allows us to compute the describing functions of the nonlinear basis. These describing functions are substituted into the matrix $\boldsymbol{M}_{11}$. Finally, the structured singular value of $\boldsymbol{M}_{11}$ can be calculated. The magnitude of pitch angle $X$ is increased until the $\mu$ value of $\boldsymbol{M}_{11}$ reaches unity. Then, the robust LCO magnitude $X^*$ can be calculated.

## 4 Numerical example

The numerical example selected to verify the above identification and modeling methods is a two-dimensional wing section with structural nonlinearity. Its physical parameters are given in Table 1 [6]. The nonlinearity considered here is a memoryless quintic gain, that affects the stiffness of the pitch motion through the pitch rotation of the airfoil. Considering the quasi-steady aerodynamic force [17], the motion equation of the wing section is written as

$$\rho U^2 b\begin{bmatrix}-c_{l\alpha}\left(\alpha+\frac{1}{U}\dot{h}+\left(\frac{1}{2}-a\right)\frac{b}{U}\dot{\alpha}\right)-c_{l\beta}\beta\\ c_{m\alpha}b\left(\alpha+\frac{1}{U}\dot{h}+\left(\frac{1}{2}-a\right)\frac{b}{U}\dot{\alpha}\right)+c_{m\beta}b\beta\end{bmatrix}$$
$$=\begin{bmatrix}m & mx_\alpha b\\ mx_\alpha b & I_\alpha\end{bmatrix}\begin{bmatrix}\ddot{h}\\ \ddot{\alpha}\end{bmatrix}+\begin{bmatrix}c_h & 0\\ 0 & c_\alpha\end{bmatrix}\begin{bmatrix}\dot{h}\\ \dot{\alpha}\end{bmatrix}$$
$$+\begin{bmatrix}k_h & 0\\ 0 & k_\alpha\end{bmatrix}\begin{bmatrix}h\\ \alpha\end{bmatrix}+\begin{bmatrix}0\\ k_{\alpha^5}\alpha^5\end{bmatrix}. \quad (24)$$

In Table 1, $k_\alpha^5$ stands for the nonlinear stiffness coefficient. For two-dimensional wing section, the first four poles of the on-line elastic modes at the velocity of 10.5 m/s were obtained from the eigenvalue solution of the characteristic matrix:

$$\begin{aligned}p_{1,2}&=-1.8856\pm \mathrm{j}17.2911,\\ p_{3,4}&=-1.2734\pm \mathrm{j}6.3344.\end{aligned} \quad (25)$$

Note that the frequency and damping ratio for each mode are identified according to the experimental data in the wind tunnel test or flight test, and the poles of these modes are derived accordingly. Nevertheless, we focused on the problems of uncertain model identification and robust LCO analysis. Without loss of generality, we obtained the poles by solving the characteristic matrix instead of estimating the poles through records of $\{u, y\}$.

As indicated in Section 2.3, these four dynamic poles were used to construct rational orthonormal basis $L_i(s)$ of the linear part $P_{12}(s)$. The order of the polynomial nonlinear basis was selected to be five to depict the unmodeled dynamics or ream nonlinearity. Note that the order can be any integer value, but it cannot be too high to avoid influencing

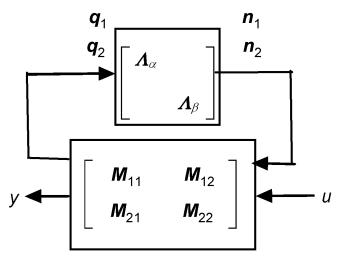


**Figure 4** LFT framework considering uncertainties and nonlinearities.

**Table 1** Parameters of the airfoil

| Parameter value | | Parameter value | |
|---|---|---|---|
| $U$ | 10.5 m/s | $a$ | –0.6 |
| $b$ | 0.135 m | $\rho$ | 1.225 kg/m$^3$ |
| $m$ | 12.387 kg | $x_\alpha$ | 0.2466 |
| $I_\alpha$ | 0.065 m$^2$kg | $k_h$ | 2844.4 N/m |
| $c_\alpha$ | 0.180 m$^2$kg/s | $c_h$ | 27.43 kg/s |
| $c_{l\alpha}$ | 6.28 | $c_{m\alpha}$ | –0.628 |
| $c_{l\beta}$ | 3.358 | $c_{m\beta}$ | –0.635 |
| $k_\alpha$ | 2.82 Nm/rad | $k_\alpha^5$ | 70 |

the identified parameters significantly. Otherwise, poor numerical results are generated. The input-output signals were generated in the time domain by the Simulink diagram in Matlab. In this numerical case, the measured output signal is the pitch angle and the input is flap angle. The sine frequency sweep input command ranges from 0 Hz to 5 Hz over 32 s, and the amplitude of the flap signals is 10° with the sample frequency fixed at 100 Hz. By using a fixed-step-size Runge-Kuta integration scheme implemented in Simulink, the output pitch angle was obtained from the airfoil's dynamics in eq. (24).

The time trace of the error signal from the identified nominal model is illustrated in Figure 5, which has a relative difference of 0.14% from the simulated dynamic error signal. From this figure, the nominal model identified by the orthonormal-base algorithm describes the aeroelastic dynamics so accurately that we cannot distinguish the nominal output from the true dynamics. However, this is an ideal case because we used the accurate poles. We cannot avoid errors when estimating natural frequencies and the damping ratio in the ground vibration test. Thus, we should consider the case that the pole error exists in the identification procedure. Here, we assumed an inaccurate pitch stiffness of $k_\alpha = 2.26$ to construct the orthonormal basis. The identified output pitch angle of the nominal Block-oriented model is denoted by the short dotted line in Figure 5. It can be seen that this model differs from the true dynamics in magnitude. At this time, the relative difference of the error signals between the nominal model and the true dynamics is 32%. It may be concluded that only using this nominal model, would misleading results be provided. The nominal model cannot account for the model error itself. Thus, we need to develop an uncertain model set identification method to describe the model error itself.

At different velocities, the one-step algorithm developed in Section 2.2 was applied to the identification of uncertain problem of the model set using the accurate poles. The optimization problem was solved by the SQP method. The indicative function value of the one-step method is 0.30%. Figure 6 illustrates the error signals by the model set identification algorithm at the velocity of 10.5 m/s. The estimated parameters are shown in Table 2. In this table, the parameters for the nominal model were identified by the least square method and SVD analysis. As described in Section 2.2, the solution approach requires that the bounds can cover the outputs, and this figure indicates that the restrictions hold. From Table 2 and Figure 6, the upper and lower bounds of the error signals are close to each other without pole errors. Meanwhile, the difference of bounds for uncertain models was small as well. The uncertain model can be used to characterize the dynamic properties for an aeroelastic system. The uncertain identification problem was considered with pole error when the pitch stiffness is not so accurate, that is, $k_\alpha = 2.26$. The bounds of the identified error signals are shown in Figure 7, and the indicative function value is 54.8%, which is much larger than that without pole error. Compared with Figure 6, the bounds of the error signals in Figure 7 are larger than those in Figure 6. However, it still covers the simulated data and thus is not distorted in describing the dynamics.

**Table 2** Parameter bounds for the uncertain model

| | Upper and lower bounds for uncertain model | Identified parameters for nominal model |
|---|---|---|
| $\alpha_1$ | [−1.4767, −1.4752] | −1.4752 |
| $\alpha_2$ | [ 2.0161, 2.0174] | 2.0174 |
| $\alpha_3$ | [−4.3377, −4.3377] | −4.3377 |
| $\alpha_4$ | [−1.9071, −1.9043] | −1.9071 |
| $\beta_1$ | [−0.0000, 0.0000] | −0.0000 |
| $\beta_2$ | [−0.0000, 0.0000] | 0.0000 |
| $\beta_3$ | [−0.0000, 0.0001] | 0.0001 |
| $\beta_4$ | [−0.0000, 0.0000] | −0.0000 |
| $\beta_5$ | [1.0000, 1.0000] | 1.0000 |

After obtaining the upper and lower bounds for the uncertain model set, we decided the model set's nominal parameters and its uncertainties according to a specified criterion. The nominal parameters and error bound for the model set are defined in eqs. (17) and (18). Consequently, the nominal LCO analysis can be conducted using the identified nominal model parameters. At a specified velocity, the nonlinear polynomial gain was derived based on the magnitude of the pitch angle. By substituting this gain into the state matrix, the magnitude for the LCO can be determined by driving the least damped eigenvalue into the imaginary axis. Figure 8 shows the relationship between the LCO velocity and magnitude of the pitch angle with different methods. In this figure, the square marker represents the magnitude by the direct time integration method. The circular marker represents the LCO magnitude by the describing method based on the accurate dynamics. The upper and lower triangular markers stand for the LCO magnitude by nominal identification and uncertain model set identification, respectively. From this figure, there is little difference between the LCO magnitude of the true dynamics and that of the identified uncertain model (the circular marker and the lower triangular marker). It may be concluded that this data-based identification method for an uncertain model set can be applied to LCO magnitude prediction of nonlinear aeroelastic system.

When the uncertain model set was generated by the data-based identification method, the LFT modeling and robust LCO analysis were conducted based on each uncertain model set at different velocities. The robust LCO magnitude was derived as shown in Figure 9, using the $\mu$ stability method presented in Section 3. From this figure, it can be seen that by considering the model error itself, the robust LCO magnitude may be less than that of the nominal model at a given speed. From the frequency of the maximum value of $\mu$, we can also obtain the frequency of possible LCO occurrence.

Consider that some errors occur while measuring the frequencies and damping ratios in the wind tunnel test, the

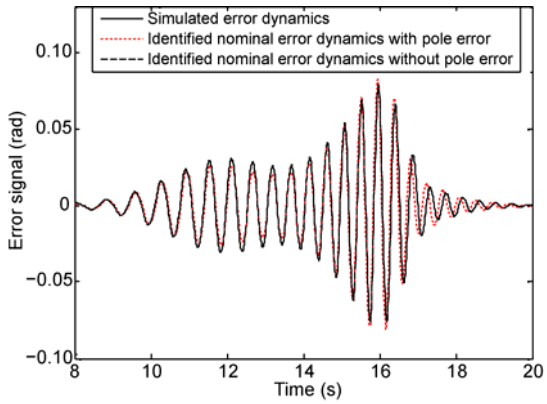


**Figure 5** Identified nominal models with and without pole errors.

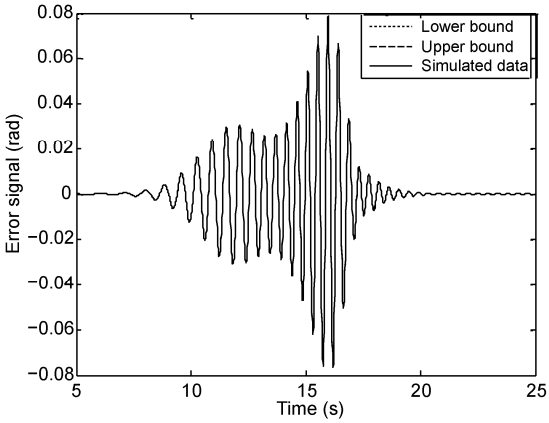


**Figure 6** Results of the uncertain model identification (without pole error).

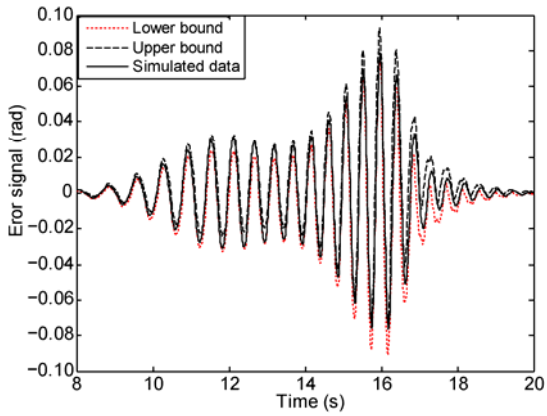


**Figure 7** Results of the uncertain model identification (with pole error).

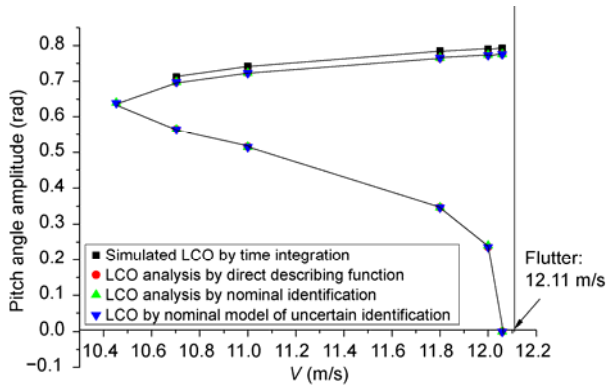


**Figure 8** Relationship between the LCO velocity and magnitude of the pitch angle.

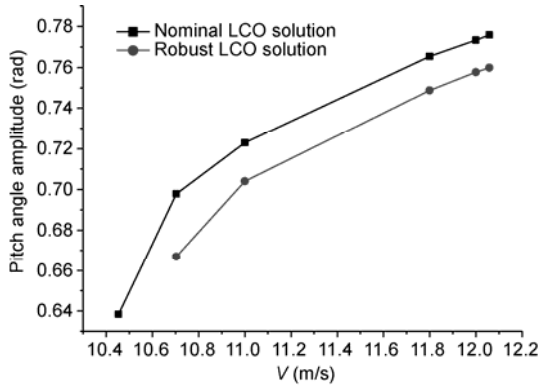


**Figure 9** Relationship between the robust LCO velocity and the magnitude of pitch angle.

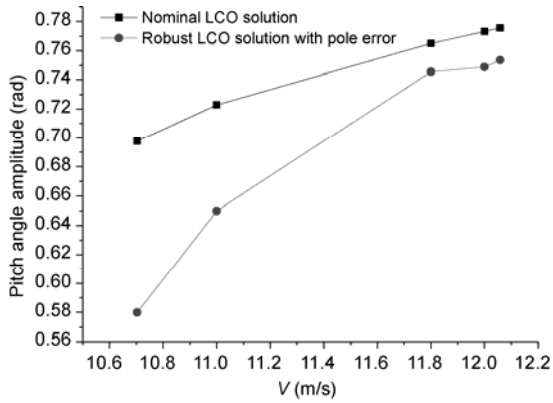


**Figure 10** Relationship between the robust LCO velocity and the magnitude of pitch angle (with pole error).

pole of the dynamic system is inaccurate in a true experiment. Thus, we considered the first two poles to have 5% errors in their imaginary parts. With these poles, we constructed the proper orthonormal basis and conducted the identification procedure again. After estimating the uncertain models with pole errors, the robust LCO analysis was performed based on $\mu$ method. The result is illustrated in Figure 10. By comparing Figure 9 with Figure 10, we can see that a lower magnitude of the pitch angle was obtained when inaccurate poles were used at a specified speed.

## 5 Conclusion

According to input-output signals, a framework for identification and robust LCO analysis was proposed in this study,

with data-based estimation and $\mu$ analysis method. The bounds of uncertain Block-oriented aeroelastic model with nonlinearity were obtained in the time domain by data-based method. And then robust LCO analysis of the identified model set was performed. An example of a two-degree wing section was carried out to validate the framework above. Results indicate that the dynamic characteristics and model uncertainties of aeroelastic system can be depicted by the data-based identification method. This framework can be effective even with inaccurate poles, which is advantageous to aeroelastic wind tunnel experiment or flight test. The numerical example indicates that the robust LCO magnitude of pitch angle for uncertain model is lower than that of nominal model at the same speed.

*This work was supported by the National Natural Science Foundation of China (Grant Nos. 90716006 and 10902006), Specialized Research Fund for the Doctoral Program of Higher Education (Grant No. 20091102110015) and the Innovation Foundation of BUAA for PhD Graduates.*

1 Doyle J C. Analysis of feedback systems with structured uncertainties. IEE Proc, Part D, 1982, 129(6): 242–250
2 Lind R, Brenner M. Analyzing aeroservoelastic stability margins using the $\mu$ method. AIAA-1998-1895, 1998
3 Wu Z G, Yang C. A new approach for aeroelastic robust stability analysis. Chin J Aeron, 2008, 21(5): 417–422
4 Yun H W, Han J L. Calculation method for robust flutter based on altitude perturbation (in Chinese). J Nanjing Univ Aeron Astron, 2007, 39(6): 731–735
5 Gu Y S, Yang Z C. Robust flutter analysis of an airfoil with flap freeplay uncertainty. AIAA-2008-2201, 2008
6 Baldelli D H, Lind R, Brenner M. Nonlinear aeroelastic/aeroservoelastic modeling by block-oriented identification. J Guid Contl Dyn, 2005, 28(5): 1056–1064
7 Zeng J, Baldelli D H, Brenner M. Novel nonlinear Hammerstein model identification: Application to nonlinear aeroelastic/ aeroservoelastic system. J Guida Contl Dyn, 2008, 31(6): 1677–1686
8 Baldelli D H, Chen P C, Liu D D, et al. Nonlinear aeroelastic modeling by block-oriented identification, 2004, AIAA 2004-1938
9 Baldelli D H, Lind R, Brenner M. Control-oriented flutter/limit-cycle-oscillation prediction framework. J Guid Contl Dyn, 2008, 31(6): 1634–1642
10 Lind R, Prazenica R J, Brenner M J. Estimating nonlinearity using volterra kernels in feedback with linear models. Nonlinear Dynamics, 2005, 39: 3–23
11 Figueroa J L, Biagiola S I, Agamennoni O E. An approach for identification of uncertain Wiener systems. Math Comput Model, 2008, 48: 305–315
12 Biagiola S I, Figueroa J L. Wiener and Hammerstein uncertain models identification. Math Comput Simul, 2009, 79: 3296–3313
13 Ninness B M, Gustafsson F. A unifying construction of orthonormal bases for system identification. Proceedings of the 33rd Conference on Decision and Control. Lake Butmavista, FL, December 1994. 3388–3393
14 Zhou T. Introduction to Control-Oriented SystemIidentification. Beijing: Tsinghua University Press, 2004
15 Baldelli D H, Mazzaro M C, Pena R S. Robust identification of lightly damped flexible structures by means of orthonormal bases. IEEE Trans Contl, Syst Technol, 2001, 9(5): 696–707
16 Baldelli D H, Lind R, Brenner M. Data-based robust match-point solutions using describing function method. 2005, AIAA-2005–1857
17 Ko J, Kurdila A J, Strganac T W. Nonlinear control of a prototypical wing section with torsional nonlinearity. J Guid Contl Dyn, 1997, 20(6): 1181–1189